Cluster versus POTENT density and velocity fields

Branchini, E; Zehavi, [No Value]; Plionis, M; Dekel, A

Published in:
Monthly Notices of the Royal Astronomical Society

DOI:
10.1046/j.1365-8711.2000.03257.x

Publication date:
2000

Mon. Not. R. Astron. Soc. **313**, 491–503 (2000)

Cluster versus POTENT density and velocity fields: cluster biasing and Ω

E. Branchini,[1,2★] I. Zehavi,[3,4] M. Plionis[5,6] and A. Dekel[4]

[1]*Department of Physics, University of Durham, South Road, Durham DH1 3LE*
[2]*Kapteyn Institute, University of Groningen, Landleven 12, 9700 AV Groningen, the Netherlands*
[3]*NASA/Fermilab Astrophysics Group, Fermi National Accelerator Laboratory, Box 500, Batavia, IL 60510-0500, USA*
[4]*Racah Institute of Physics, The Hebrew University, Jerusalem 91904, Israel*
[5]*National Observatory of Athens, Lofos Nimfon, Thesio, 18110 Athens, Greece*
[6]*SISSA – International School for Advanced Studies, via Beirut 2-4, I-34013 Trieste, Italy*

Accepted 1999 November 8. Received 1999 October 15; in original form 1997 April 18

ABSTRACT

The density and velocity fields as extracted from the Abell/ACO clusters are compared with the corresponding fields recovered by the POTENT method from the Mark III peculiar velocities of galaxies. In order to minimize non-linear effects and to deal with ill-sampled regions, we smooth both fields using a Gaussian window with radii ranging between 12 and $20\,h^{-1}$ Mpc. The density and velocity fields within $70\,h^{-1}$ Mpc exhibit similarities, qualitatively consistent with gravitational instability theory and a linear biasing relation between clusters and mass. The random and systematic errors are evaluated with the help of mock catalogues. Quantitative comparisons within a volume containing ~12 independent samples yield $\beta_c \equiv \Omega^{0.6}/b_c = 0.22 \pm 0.08$, where b_c is the cluster biasing parameter at $15\,h^{-1}$ Mpc. If $b_c \sim 4.5$, as indicated by the cluster correlation function, our result is consistent with $\Omega \sim 1$.

Key words: galaxies: clusters: general – galaxies: kinematics and dynamics – cosmology: theory – large-scale structure of Universe.

1 INTRODUCTION

The basic hypothesis underlying the study of large-scale structure is that it grew out of initial fluctuations via gravitational instability (GI). In the linear regime, this theory predicts a relation between the peculiar velocity and density fluctuation fields, $\nabla \cdot \boldsymbol{v} = -f(\Omega)\delta$, with $f(\Omega) \simeq \Omega^{0.6}$. From observations we can deduce the density field of galaxies or clusters rather than the density field of the underlying matter distribution. One then needs to assume a relation between the galaxy or cluster fluctuation field and that of the mass. A first order approximation is that of a linear 'biasing' relation (hereafter LB) in which the two fields, smoothed on the same scale, obey the relation $\delta_o = b_o\delta$. Thus, GI+LB boil down to a simple relation between observables,

$$\nabla \cdot \boldsymbol{v} = \beta_o \delta_o, \qquad \beta_o \equiv \Omega^{0.6}/b_o. \tag{1}$$

The density field of the extragalactic objects can be derived from a whole-sky redshift survey, while the velocity divergence can be reconstructed from a sample of redshifts and distances inferred by Tully–Fisher-like distance indicators. Therefore, combining these data allows a measurement of β_o, which, subject to some a priori knowledge of the biasing parameter b_o, provides constraints on the cosmological density parameter Ω. A related analysis, invoking the integral of equation (1), can be performed using velocities rather than densities.

The efforts to measure β from various data sets using different methods are reviewed in e.g. Dekel (1994, 1997) and Strauss & Willick (1995). The most reliable density–density analysis, incorporating certain mildly non-linear corrections, is the recent comparison of the *IRAS* 1.2-Jy redshift survey and the Mark III catalogue of peculiar velocities yielding, at Gaussian smoothing of $12\,h^{-1}$ Mpc, $\beta_{IRAS} = 0.89 \pm 0.12$ (Sigad et al. 1998, hereafter PI98, replacing an analysis of earlier data by Dekel et al. 1993). An analysis of optical galaxies has provided a somewhat lower value for β_{opt} (Hudson et al. 1995), in accordance with the expected higher biasing parameter for early-type galaxies as demonstrated by their stronger clustering (cf. Lahav, Nemiroff & Piran 1990). Recent velocity–velocity comparisons typically yield values of $\beta_{IRAS} \simeq 0.5$–0.6 ± 0.1 (Davis, Nusser & Willick 1996; Willick et al. 1997b and references therein; da Costa et al. 1998; Willick & Strauss 1998; Branchini et al. 1999). The main source of uncertainty in the interpretation of the β estimates arises from our ignorance concerning the biasing relations. Fortunately, we do have a handle on the *relative* biasing parameters, based, for example, on the relative amplitudes of the correlation functions of the different types of objects, which should scale like b^2. Since different classes of extragalactic objects are assumed to trace the same velocity field, one can hope to tighten the constraints on Ω by deriving β for several different types of objects.

★ E-mail: branchin@astro.rug.nl

Clusters of galaxies are promising candidates for this purpose because they are well-defined objects and are sampled quite uniformly to large distances, much larger than the available galaxy peculiar velocity samples. The use of the cluster distribution to probe the large-scale dynamics has been mainly restricted to dipole analyses, where the predicted velocity at the Local Group (LG) is compared with its observed motion relative to the cosmic microwave background (CMB) frame (Plionis & Valdarnini 1991, hereafter PV91; Scaramella, Vettolani & Zamorani 1991; Plionis & Kolokotronis 1998). It has been found that the directions of the two dipoles converge when using a large enough sample of clusters ($>150\,h^{-1}$ Mpc), as expected from the assumed global homogeneity of the cosmological model (and contrary to the finding of Lauer & Postman 1994, based on their attempt to measure directly peculiar velocities for clusters). Once the cluster distribution is properly corrected from redshift to real space, the corresponding value of β derived from the dipole is $\beta_c \simeq 0.21$ (Branchini & Plionis 1995, 1996, hereafter BP96; Branchini, Plionis & Sciama 1996; Scaramella 1995a). This estimate is higher than the value derived without this correction (Scaramella et al. 1991; PV91), and is consistent with $\Omega \sim 1$ for a cluster biasing parameter of $b_c \sim 4$–5 as indicated by the cluster correlation analyses. The validity of the LB assumption for clusters might be questioned. In particular, such a large biasing parameter cannot follow the linear relation in deep underdensities. However, because of their low number density, clusters trace the underlying mass density field with a large inherent smoothing scale set by their mean separation. This has the effect of decreasing the density contrast and restoring the plausibility of the LB hypothesis over a large fraction of the volume sampled.

It turns out that the bulk motion, as predicted from the cluster distribution with $\beta_c \sim 0.2$ inside a sphere of radius $\sim 50\,h^{-1}$ Mpc about the LG, is consistent with that derived directly from galaxy peculiar velocities (see Dekel 1997; Dekel et al. 1999; Giovanelli et al. 1996, 1998a, 1998b). However, the estimate of β_c from the dipole at one point, or from the bulk flow, naturally suffers from severe cosmic scatter (e.g. Juskiewicz, Vittorio & Wyse 1990). The cosmic scatter can be reduced if the comparison is made at several independent points. Branchini (1995) and Plionis (1995) have attempted to compare predicted velocities from the cluster distribution with observed peculiar velocities of groups and clusters from Tormen et al. (1993), Hudson (1994) and Giovanelli et al. (1997), obtaining again $\beta_c \sim 0.2$. These analyses, however, are of limited validity because they compare smoothed and unsmoothed velocities.

The purpose of this work is to measure β_c by comparing the Abell/ACO cluster distribution and the galaxy peculiar velocities of the comprehensive Mark III catalogue as analysed by POTENT. The comparison is performed alternately at the density–density and the velocity–velocity levels, and involves a careful error analysis. In Section 2 we summarize the Mark III data, the POTENT method and the associated errors. In Section 3 we describe the reconstruction of the cluster density and velocity fields and the various sources of error. In Section 4 we perform a quantitative comparisons of the cluster and POTENT fields, in order to determine β_c. We conclude our results in Section 5.

2 POTENT RECONSTRUCTION FROM PECULIAR VELOCITIES

The POTENT procedure recovers the underlying mass–density fluctuation field from a whole-sky sample of observed radial peculiar velocities. The steps involved are

(i) preparing the data for POTENT analysis, including grouping and correcting for Malmquist bias,

(ii) smoothing the peculiar velocities into a uniformly smoothed radial velocity field with minimum bias,

(iii) applying the ansatz of gravitating potential flow to recover the potential and three-dimensional velocity field, and

(iv) deriving the underlying density field by an approximation to GI in the mildly non-linear regime.

The POTENT method, which grew out of the original method of Dekel, Bertschinger & Faber (1990, hereafter DBF), is described in detail in Dekel et al. (1999, hereafter D99) and is reviewed in the context of other methods by Dekel (1997, 1998). Further improvements since DBF have been introduced, which we use in the present analysis. They are discussed in detail by Sigad et al. (1998).

We use the Mark III catalogue of peculiar velocities (Willick et al. 1995, 1996, 1997a), which is a careful compilation of several data sets consisting of ~3000 spiral and elliptical galaxies. The non-trivial procedure of merging the data sets accounts for differences in the selection criteria, the quantities measured, the method of measurement and the Tully–Fisher (hereafter TF) calibration techniques. The data per galaxy consist of a redshift z and a 'forward' TF (or D_n–σ) inferred distance, d. The radial peculiar velocity is then $u = cz - d$. This sample enables a reasonable recovery of the smoothed dynamical fields in a sphere of radius $\sim 50\,h^{-1}$ Mpc about the Local Group, extending to $\sim 70\,h^{-1}$ Mpc in some well-sampled regions.

The POTENT method is evaluated using mock catalogues. The mock catalogues and the underlying N-body simulation are described in detail in Kolatt et al. (1996, hereafter K96). Here we only stress that a special effort was made to generate a simulation that mimics the actual large-scale structure in the real Universe, in order to take into account any possible dependence of the errors on the signal.

2.1 Errors in the POTENT reconstruction

D99 and PI98 demonstrate how well POTENT can perform with ideal data of dense and uniform sampling and no distance errors. The reconstructed density field, from input that consisted of the exact, G12-smoothed radial velocities, is compared with the true G12 density field of the simulation. The comparison is carried out at grid points of spacing $5\,h^{-1}$ Mpc inside a volume of effective radius $40\,h^{-1}$ Mpc. No bias is introduced by the POTENT procedure itself and they find a small scatter of 2.5 per cent that reflects the accumulating effects of small deviations from potential flow, scatter in the non-linear approximation and numerical errors.

Using the mock catalogues described by K96, we want to check and quantify how well the POTENT reconstruction method works on our sparse and noisy data. Our goal is eventually to compare the POTENT fields to the density and velocity fields obtained from the distribution of clusters. As the clusters are sparse tracers of the mass, we also need to explore smoothing radii larger than the G12 (commonly used in POTENT applications), and we check the G15 and G20 cases as well. The errors caused by sparse sampling and non-linear effects are expected to be smaller for the larger smoothing scales, while the sampling-gradient bias may increase.

For each smoothing radius, we execute the POTENT algorithm

on each of the 20 noisy mock realizations of the Mark III catalogue, recovering 20 corresponding density and velocity fields. We will later consider the individual fields as well as the mean fields averaged over the mock catalogues. The error in the POTENT density field at each point in space, σ_{δ_p}, is taken to be the rms difference over the realizations between δ_p and the true density field of the simulation smoothed on the same scale. The errors on the smoothed velocity fields, σ_{v_p}, are estimated by a similar procedure from the Y supergalactic component of the mock velocity field. We evaluate the density and the velocity fields and their errors at the points of a Cartesian grid with $5\,h^{-1}$ Mpc spacing. In the well-sampled regions, with the G15 smoothing, the errors for the density are typically $\sigma_{\delta_p} \approx 0.1$–$0.3$ and $\sigma_{v_p} \approx 50$–$250\,\mathrm{km\,s^{-1}}$, but they are much larger in certain regions at large distances.

The error estimates σ_{δ_p} and σ_{v_p} are two of the criteria used to exclude the noisy regions from the comparison with the clusters. A third one is the distance from the fourth neighbouring object in the Mark III catalogue, R_4, which provide us with a measure of the poor sampling in the parent velocity catalogue. Two more cuts have been applied on the cluster density and velocity fields, using the errors σ_{v_c} and σ_{δ_c} obtained from the mock catalogues analysis in Section 3.3.2. Furthermore, we only consider objects within $R = 70\,h^{-1}$ Mpc and outside the Zone of Avoidance ($|b| > 20°$). Our last constraint is on the misalignment angle between the cluster and the POTENT velocity vectors, $\Delta\theta$, which we impose to be smaller than 45°. The rationale behind such an additional cut is that we are assuming all along LB as a working hypothesis. This predicts, for ideal data, that the velocity vectors reconstructed from the distribution of the clusters should be aligned with the velocity vectors of mass deduced by POTENT. However, the various random errors and systematics in both types of real data analysed here cause deviations from this simple picture. In our 'standard comparison volume' we restrict the comparison only to points where the velocity vectors of the POTENT and cluster fields are broadly aligned with each other. Note that the misalignment constraint may, in principle, affect our β estimate and therefore it will be dropped in some of the robustness tests performed in Section 4.4 and Section 4.5. A 'standard comparison volume' is defined through the set of cuts reported in Table 1. The two cuts σ_{v_p} and σ_{v_c} turned out to be ineffective, in the sense that they are redundant for reasonable choices of the other parameters, and were not implemented. The σ_{δ_c} constraint is obtained by scaling σ_{δ_p} by the β_c of BP96. For the sake of consistency, we perform all tests with the mock catalogues using the same standard cuts, even though the $\Delta\theta$ cut does not affect the δ–δ comparison. The standard volume, V_{st}, depends on the smoothing applied. A Gaussian filter of $15\,h^{-1}$ Mpc has an effective radius $R_e \sim 38\,h^{-1}$ Mpc [defined by $(4\pi/3)R_e^3 = V_{st}$]. The rms of σ_{δ_p} there is $\sim$0.18 and that of σ_{v_p} is $\sim 150\,\mathrm{km\,s^{-1}}$. Finally, note that the misalignment criterion depends on the the particular velocity field of the generic mock catalogue and therefore the same standard cuts define slightly different comparison volumes in each of the mock Mark III and cluster catalogues tested.

In what follows we will present the results as the average of the individual results obtained for each catalogue, and for illustrative purposes also show the results obtained for the mean fields, averaged over the mock catalogues. (The volumes corresponding to the individual mock catalogues typically share 80 per cent of their points with the volume defined for the average fields). Some of these errors are systematic. The systematic errors can be evaluated by inspecting the average of results over the mock

Table 1. The standard cuts. Column 1: σ_{δ_p}, maximum error in POTENT δ; column 2: σ_{δ_c}, maximum error in cluster δ; column 3: R_4, maximum distance from the fourth neighbouring object in h^{-1} Mpc; column 4: R, maximum radius in h^{-1} Mpc; column 5: $|b|$, minimum galactic latitude in degrees; column 6: $\Delta\theta$, maximum misalignment in degrees.

σ_{δ_p}	σ_{δ_c}	R_4	$\lvert b\rvert$	R	$\Delta\theta$
0.3	1.43	13	20°	70	45°

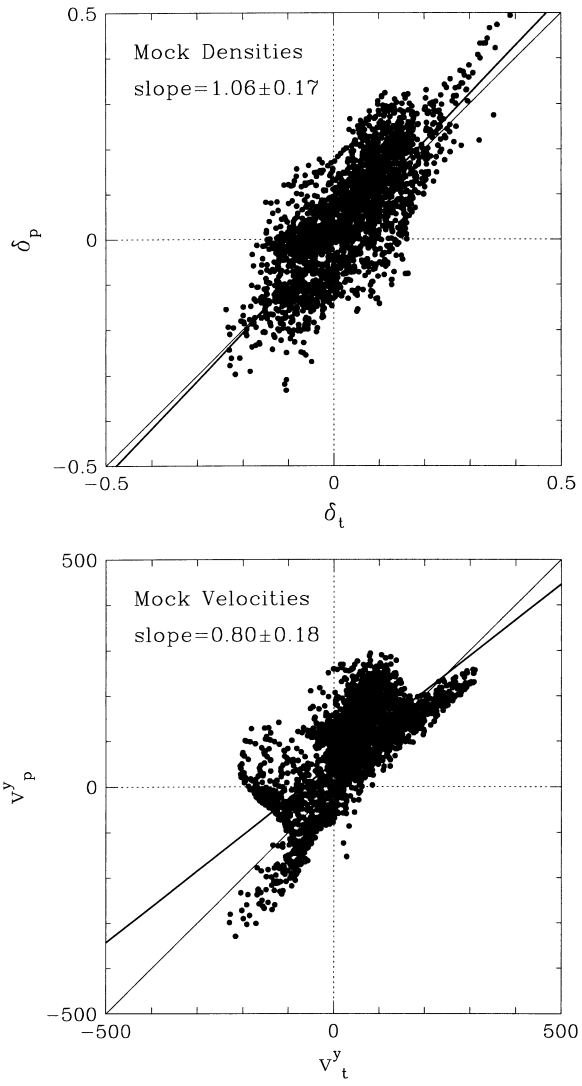

Figure 1. Systematic errors in the POTENT analysis. The POTENT fields recovered from the noisy and sparsely sampled mock data are compared with the 'true' G15 fields of the simulation. The comparison is at uniform grid points within our 'standard comparison volume' of effective radius $40\,h^{-1}$ Mpc. Plotted, in both cases, is the POTENT field averaged over the 20 realizations. The heavy solid lines and the slopes quoted refer to the average (and standard deviation) of the best fig from the 20 realizations. Top: the POTENT density field versus the true density field. Bottom: the POTENT supergalactic Y component of the velocity field versus the true velocities in the simulation.

catalogues or by comparing directly the average POTENT density and velocity fields with the underlying smoothed fields of the simulation. The top panel of Fig. 1 shows this comparison for the G15 smoothed density fields, at the points of a uniform grid inside the standard volume. The residuals in this scatter plot ($\langle\delta_{\rm p}\rangle$ versus $\delta_{\rm t}$) are the local systematic errors. Their rms value over the standard volume is 0.08. The corresponding rms of the random errors ($\delta_{\rm p}$ versus $\langle\delta_{\rm p}\rangle$) is 0.16. The systematic and random errors add in quadrature to give the total error ($\delta_{\rm p}$ versus $\delta_{\rm t}$), the rms of which over the realizations at each point, $\sigma_{\rm p}$, is used in the analysis below.

To quantify the effect of these errors on the determination of β we perform a regression of $\delta_{\rm p}$ on $\delta_{\rm t}$, for each mock catalogue and for the average field, by minimizing the following χ^2:

$$\chi^2 = \sum_{i=1}^{N_{\rm tot}} \frac{(\delta_{{\rm p},i} - A - B\delta_{{\rm t},i})^2}{\sigma^2_{\delta_{\rm p},i}}. \qquad (2)$$

The figure shows no considerable systematic deviations from the $\delta_{\rm p} = \delta_{\rm t}$ line (the slope of the regression for the average field comes out as 1.01). The average of the slopes over the 20 mock realizations is slightly deviant from unity, 1.06, with a standard deviation of 0.17. For the other smoothings G12 and G20, in the standard comparison volume, the average of slopes is 1.06 ± 0.09 and 0.98 ± 0.28, respectively. For other choices of the cuts (see Sections 4.4 and 4.5 for some illustrative examples) the slope changes by a couple of per cent, e.g., for G15, the typical deviation from unity is by up to $\sim$5 per cent in either direction. Finally, only negligible zero-point offsets have been detected in all of the above comparisons. These results indicate that the final systematic errors are scarcely correlated with the signal or with themselves, contributing no significant bias in comparisons with density from redshift surveys.

An analogous comparison has been performed between the supergalactic Y components of the velocity fields at the same points. We limit our analysis to this component only as it is the one least affected by the uncertainties of the mass distribution near the galactic plane in the forthcoming comparison with cluster velocities. Using the two remaining Cartesian components would require an estimate of possible systematic errors that are uncertain for the cluster case (see Section 3.3.2). The bottom panel of Fig. 1 shows the corresponding scatter diagram of the average field versus the underlying one, again with G15 smoothing in the standard volume. The rms value of the residuals over the comparison volume, which represent the local systematic error, ($\langle v_p\rangle$ versus v_t), is $75\,{\rm km\,s^{-1}}$. The rms value of the random errors around the average, (v_p versus $\langle v_p\rangle$), is $130\,{\rm km\,s^{-1}}$.

Visual inspection of the figure shows clear signs of systematic errors. The peculiar morphology in the velocity–velocity scatter plot reflects correlated velocities within individual cosmic structures. Indeed, the coherence length of the velocity field is much larger than for the density field, leading to oversampling and correlations among the errors. The overall effect on the slope is a bias toward smaller values than unity. The slope of the best-fitting line for the average field is in this case 0.81, and the average of slopes over the mock catalogues reflects this as well, giving an average slope of 0.80 ± 0.18. The average slope is 0.93 ± 0.13 for the G12 case, and 0.76 ± 0.31 for G20. When varying the comparison-volume, in the G15 case, the bias is typically 12–22 per cent. Thus, the velocity comparisons tend, in general, to be less robust than the density comparisons and also more sensitive to the smoothing scale. This is probably partly caused by the larger cosmic scatter in the velocity field, larger systematic biases in the POTENT analysis (in particular the window bias and the sampling-gradient bias), which become more severe for large smoothing scales, and correlation among the errors.

The POTENT output of the real Mark III data is similarly provided, for the three different smoothings, on a Cartesian grid of spacing $5\,h^{-1}\,{\rm Mpc}$, within a volume of radius $80\,h^{-1}\,{\rm Mpc}$. The errors at each grid point ($\sigma_{\delta_{\rm p}}$ and $\sigma_{v_{\rm p}}$) are taken to be the error estimates of the mock catalogues detailed above, i.e. the rms difference over the realizations between the recovered fields and the true underlying one.

3 RECONSTRUCTING THE CLUSTER DENSITY AND VELOCITY FIELDS

The present analysis is based on the real-space cluster distribution and peculiar velocities recovered from the observed distribution of Abell/ACO clusters in redshift space. The details of our reconstruction method are described in BP96. Here we briefly describe the data and sketch the main features of the procedure including the error analysis. It is worth noticing that in the present comparison with POTENT we are mainly interested in a local region of radius $\sim 70\,h^{-1}\,{\rm Mpc}$, where the reconstruction technique is more reliable than at larger distances.

3.1 Cluster data

The cluster sample used in BP96 contains all the Abell and ACO clusters (Abell 1958; Abell, Corwin & Olowin 1989) of richness class $R \geqslant 0$ within $250\,h^{-1}\,{\rm Mpc}$, $|b| \geqslant 13°$ and $m_{10} \leqslant 17$ (where m_{10} is the magnitude of the tenth brightest cluster galaxy as corrected in PV91). The Abell and ACO catalogues were unified into a statistically homogeneous whole-sky sample of clusters using the distance-dependent weighting scheme of P91. The sample used in this work contains the same $\sim$500 clusters, for which 96 per cent now have measured redshifts, most recently from the ESO Nearby Abell Cluster Survey (ENACS: Katgert et al. 1996). For the remaining $\sim$20 clusters the redshifts were estimated from the m_{10}–z relation calibrated as in PV91. The results from this improved sample turn out to be fully consistent with the original ones of BP96.

3.2 Reconstruction of uniform cluster catalogues in real space

Our reconstruction procedure consists of two steps. First, Monte Carlo techniques are used to correct for observational biases and return a whole-sky distribution of clusters in redshift space. Then, this distribution is fed into an iterative reconstruction procedure (similar in spirit to Yahil et al. 1991) which assumes linear GI + LB to recover the real-space positions and peculiar velocities of the clusters.

The main observational biases arise from a systematic mismatch between the Abell and ACO catalogues, and from the latitude-dependent Galactic obscuration; the radial selection is not an issue because it is quite uniform in the volume relevant for our analysis. To minimize the possible systematic errors in the model cluster velocity field we need to unify the Abell and ACO catalogues into a statistically homogeneous whole-sky sample of clusters. We obtain this by using the distance-dependent weighting scheme of PV91 which enforces the same number density in

equal-volume shells for the two cluster populations. The number of radial shells is left as a free parameter. To correct for Galactic obscuration, we generate a set of cluster catalogues of uniform sky coverage, by adding a population of synthetic clusters. The Galactic obscuration at $|b| \geqslant 20°$ is modelled by a cosecant law, $\mathcal{P}(b)$. As in BP96, we have chosen two different sets of absorption coefficients to account for observational uncertainties. Synthetic clusters are added with a probability proportional to $\mathcal{P}(b)$ such that they are spatially correlated with the real clusters according to the observed cluster–cluster correlation function. Within the Zone of Avoidance (ZoA), $|b| < 20°$, the volume is filled with synthetic clusters, in bins of redshift and longitude, by cloning the cluster distribution in the adjacent latitude strips outside the ZoA. Both real and synthetic Monte Carlo generated clusters are mass weighted to determine the density field to be used in equation (3) below. The mass of each real cluster is proportional to the number of galaxies per cluster listed in the Abell catalogue. The mass of synthetic clusters is set equal to the mass of the real ones.

The redshift-space distortions are corrected by an iterative procedure based on linear theory and linear biasing. Equation (1) can be inverted to yield

$$\boldsymbol{v} = \frac{\beta_c}{4\pi} \int \mathrm{d}^3x' \frac{\delta(\boldsymbol{x}')(\boldsymbol{x}' - \boldsymbol{x})}{|\boldsymbol{x}' - \boldsymbol{x}|^3}. \quad (3)$$

This is used, in each iteration, to compute the radial peculiar velocities of the individual clusters, u, in the LG frame, and correct for their real distances, r, via $r = cz - u$. To avoid strong non-linear effects, the force field generated by the point-mass clusters is smoothed by a top-hat window of radius $15\,h^{-1}\,\mathrm{Mpc}$, chosen to be comparable to the cluster–cluster correlation length (see BP96). A meaningful comparison with POTENT, in view of the large mean separation between clusters ($\sim 25\,h^{-1}\,\mathrm{Mpc}$), requires that we smooth further the density and velocity fields. As input to this procedure one has to assume a value for β_c, which affects the peculiar velocities but has only a weak effect on the real-space distance as long as β_c is in the right ballpark (see BP96). We have assumed $\beta_c = 0.21$ based on matching the dipoles of the CMB and the cluster distribution (e.g. BP96).

3.3 Errors in the cluster positions and velocities

Ideally, we would also like to implement the same POTENT error assignment procedure for the cluster case. However, intrinsic difficulties in modelling the Abell/ACO selection criteria hamper the compilation of mock cluster catalogues from the K96 simulation. This problem is made worse by the size of the N-body computational, volume which is smaller than the one spanned by the real cluster population. We choose instead to evaluate cluster errors using a hybrid scheme consisting of the following.

(i) A Monte Carlo procedure of adding synthetic clusters and varying the parameters is also used to estimate the random and systematic errors that arise both from the uncertainties in modelling the observational biases and the approximations in the reconstruction.

(ii) A mock catalogue analysis, similar to the one used to assess the POTENT errors, is implemented to quantify the additional random errors that arise from the sparseness of the cluster sampling.

3.3.1 Monte Carlo analysis

The reconstruction procedure depends on a number of parameters that are only weakly constrained by observational data or theoretical arguments, such as the galactic absorption coefficients, the force smoothing length, and the weighting scheme used to homogenize the Abell and ACO catalogues. BP96 evaluated the sensitivity of the derived density and velocity fields to these parameters by allowing the parameters to vary about the standard set defined in their table 2.

The total uncertainties in the cluster positions and in the radial velocities, estimated in the CMB frame, arise from several different sources.

(i) Intrinsic errors of the reconstruction procedure, which we estimate by the standard deviation of the cluster distances over 10 Monte Carlo realizations of the same choice of parameters.

(ii) Observational errors, accounting for the freedom in the values of the free parameters, which we estimate by the standard deviation of the distances over reconstructions with different sets of values for the parameters.

(iii) Shot-noise error (equation 20 of BP96), caused by the uncertainty in the mass per cluster, which we assume proportional to the number of galaxies listed in the Abell catalogue (see BP96). This error is estimated to be of $\sim 70\,\mathrm{km\,s^{-1}}$ (one-dimensional). The shot-noise resulting from the sparseness of the mass tracers will be estimated numerically in Section 3.3.2.

(iv) Weight uncertainty. This error accounts for uncertainties in the relative weighting of Abell versus ACO clusters to correct for systematic differences between these catalogues. For this purpose, we have performed 10 different reconstructions in which the weights were randomly scattered about the standard weights of BP96 (their equation 5), following a Gaussian distribution of width that equals the Poisson error in the relative number densities of Abell and ACO clusters at every given distance. The estimated typical weight uncertainty turns out to be $\sim 85\,\mathrm{km\,s^{-1}}$.

(v) Projection uncertainty. A worry when using the Abell/ACO clusters for statistical purposes is the contamination of cluster richness caused by projection of foreground and background galaxies (e.g. Dekel et al. 1989 and references therein). The resulting uncertainty in the galaxy count per cluster has recently been estimated (Mazure et al. 1996 using the ENACS survey; Van Haarlem, Frenk & White 1997, using N-body simulations) to be ~ 17 per cent. To translate this error into a distance error, we have performed 10 reconstructions where the cluster richness was randomly perturbed by a 17 per cent Gaussian, yielding an error of $\sim 80\,\mathrm{km\,s^{-1}}$.

An upper bound to the total error for each Abell/ACO cluster can be estimated by adding in quadrature all the above errors, as if they are all independent. This results in an average error of $254\,\mathrm{km\,s^{-1}}$, with a large spread of $\pm 117\,\mathrm{km\,s^{-1}}$. If we add in quadrature only the observational, intrinsic and shot-noise errors, which are independent of each other, the average error drops only to $218\,\mathrm{km\,s^{-1}}$, indicating that our upper bound is not a great overestimate of the true error. Fig. 2 shows the distribution of the total reconstruction errors in the line-of-sight component of the peculiar velocities for the ~ 500 clusters of our subsample. Unlike the intrinsic ones, observational, shot-noise, weighting and projection errors are isotropic. Therefore, they are also representative of the uncertainties along the supergalactic Y component of the velocity fields and they will be used to estimate the cluster velocity errors σ_{vc} in Section 3.4.

For the comparison with POTENT we should identify the regions where the reconstruction from clusters is reliable. The errors are naturally larger in regions where the fraction of observed clusters

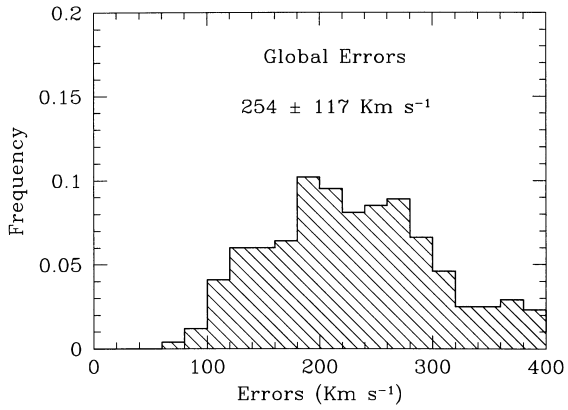

Figure 2. Histograms of the global random + systematic errors from the Monte Carlo analysis. The plot shows the frequency of the uncertainties in the line-of-sight component of the reconstructed cluster velocities. Units are $\mathrm{km\,s^{-1}}$.

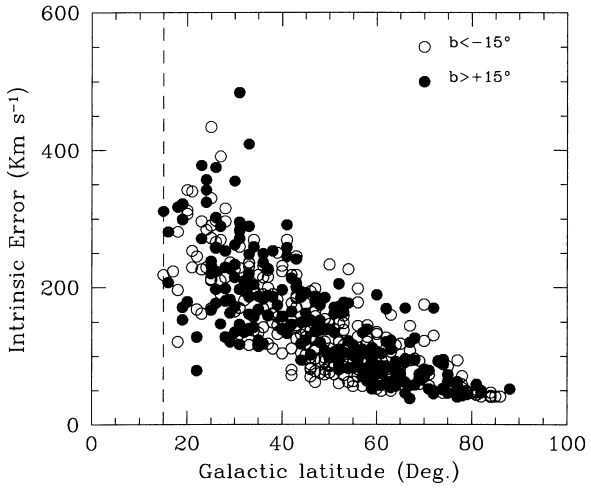

Figure 3. Environmental dependence of Monte Carlo errors. Dependence of the intrinsic errors on galactic latitude. Abell/ACO clusters in the northern galactic hemisphere are shown as filled dots, while open dots represent southern clusters.

is lower. This effect is clearly seen when we plot the intrinsic error per cluster as a function of Galactic latitude (Fig. 3). As expected, no radial dependence has been detected for the errors within the volume used for the present analysis.

3.3.2 Mock catalogue analysis

Owing to their low number density, clusters of galaxies sparsely sample the underlying density and velocity fields. This introduces an intrinsic scatter, sometimes also termed 'shot noise', when comparing the cluster and the mass fields. This is closely related to the expected scatter from the stochasticity in the bias relation (e.g. Dekel & Lahav 1999). This sort of random error is not included a priori in our cluster error estimates, but needs to be accounted for in the actual comparisons of the clusters fields with the POTENT reconstructions.

We further assess the reliability of the cluster fields, and obtain a crude estimate of the additional scatter, using the same *N*-body simulation that was the basis for the Mark III mock catalogues. In the present case, however, we obtain just one mock catalogue of clusters from the simulation. We use a friends-of-friends algorithm

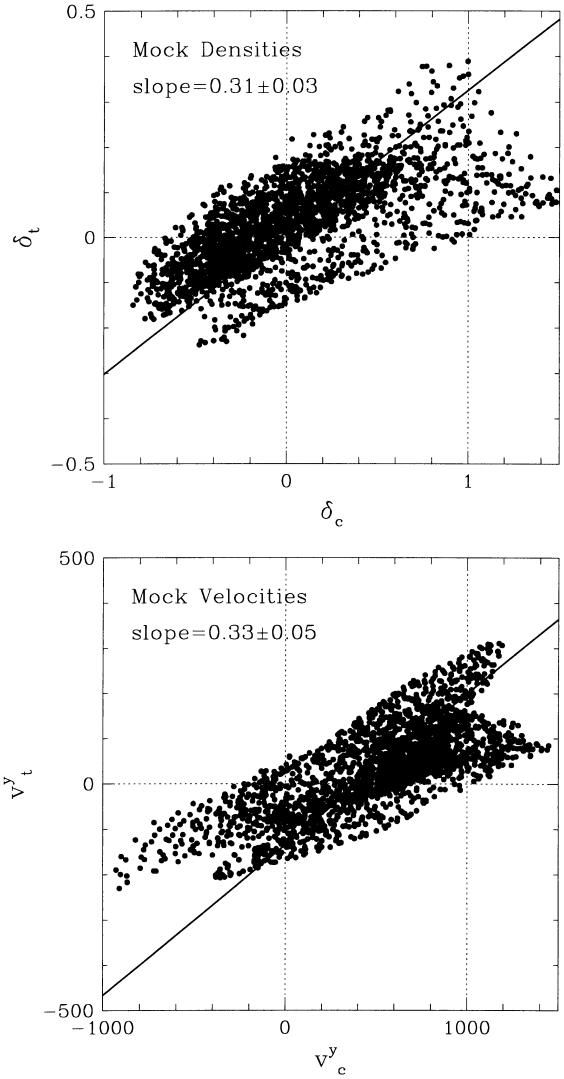

Figure 4. Random errors in the cluster mock analysis. Cluster mock density and velocity fields are obtained from the clusters identified in the K96 *N*-body simulation and compared with the underlying fields, all with G15 smoothing. The comparison is at the same points shown in Fig. 1. Top: δ–δ comparison. Bottom: v_y–v_y comparison. The solid lines correspond to the average best-fitting lines. The scatter about the fitting lines is an estimate of the intrinsic scatter in the cluster fields.

to identify groups among the particles in the simulation. The richest groups above some threshold, fixed so as to have the same number density as the Abell/ACO clusters, are identified as the mock clusters. To mimic the properties of the real cluster distribution we need to extend our mock sample out to $250\,h^{-1}$ Mpc. As this exceeds the size of the simulation, we obtain the mock cluster distribution by duplicating the clusters within the computational box using the periodic boundary conditions. The peculiar velocities from clusters are then computed from equation (3) and both the cluster density and the velocity fields are smoothed at the points of a cubic grid with $5\,h^{-1}$ Mpc spacing. The smoothed cluster fields are then compared with the true underlying fields of the simulation, smoothed on the same scale. Under the GI+LB assumptions, the fields are simply related by the biasing factor between clusters and mass in the simulation, both in the density case and for the velocities (for our $\Omega = 1$ simulation). We use the same 'standard comparison volume' considered for the POTENT

versus true comparisons and used later for the POTENT versus cluster comparisons. Fig. 4 shows the results for the G15 case.

The slopes of the best-fitting lines for the δ–δ comparison (0.32, top panel) and the v_y–v_y comparison (0.30, bottom panel) have been estimated by assigning equal weight to all points. They are a measure of the relative biasing between clusters and mass (b_c^{-1}, when regressing clusters on true fields).

The average value of the 20 volumes defined by the POTENT mock catalogues with the same criteria is 0.31 ± 0.03 for the density fields and 0.33 ± 0.05 for the velocities. For general variations in the comparison volume, values of 0.30–0.38 are typically obtained, with a slight tendency of the values obtained from velocities to be higher than those obtained from densities, within this range. Unlike the POTENT analysis in Section 2.1, we do not know the 'true' expected slope for the mock clusters and this sort of comparison is in practice a way to define it. Variations between the values obtained from densities and velocities may arise because of the larger cosmic scatter for the velocities and uncertainties in modelling the cluster distribution outside the computational volume. Another possible cause for the mismatch is the already mentioned strong correlation between the errors in the v_y–v_y analysis. Note that the difference between the slopes obtained from the δ–δ and v_y–v_y is smaller than the outcome of the POTENT analysis in Section 2.1, meaning that the various error sources affecting the v_y–v_y comparison tend to compensate each other.

The distribution of the distant clusters may significantly affect the cluster velocities, while it is almost irrelevant when computing the smoothed density field within $70\,h^{-1}$ Mpc. We therefore regard $b_c^{-1} = 0.31$ as the 'true' value for the G15 standard case. Similar values are obtained for $b_c{}^{-1}$ with the other smoothing scales.

A considerable scatter about the regression lines is found in both the δ–δ and the v_y–v_y comparisons. As the clusters in this case are free from the observational and modelling errors, this scatter is a manifestation of the additional inherent scatter in the cluster fields mentioned above. For G15, the detected scatter is $\sigma_\delta{}^{\rm int} = 0.36$ in the density case and $\sigma_v{}^{\rm int} = 300\,{\rm km\,s^{-1}}$ for the velocities. The change with smoothing scale is as expected: for G12 the scatter is larger (0.46 and 400, for densities and velocities, respectively) and for G20 the scatter is smaller (0.24 and 200). These estimates are quite robust to changes in the comparison volume.

In what follows, we adopt these dispersions as a measure of the intrinsic scatter of the cluster fields, for the POTENT–cluster mock tests in Section 4.2, and also for the comparisons with real data. The drawback of the latter assumption is the fact that the mock clusters do not accurately match the Abell/ACO cluster distribution. Most of the mock clusters do not correspond on a one-to-one basis to the Abell/ACO ones, and are less spatially correlated. Furthermore, because the mock clusters are identified from a simulation based on *IRAS* galaxies, which tend to avoid high-density regions, they might represent density peaks of a systematically lower amplitude with respect to those of the Abell/ACO clusters. Finally, the dissimilarity could be even more severe for the velocity calculations because of the duplication procedure adopted outside the *N*-body computational volume. Still, not having a better way to determine accurately this scatter for the real data, and understanding that its magnitude mainly depends on the sparseness of clusters and smoothing adopted, we believe that our approach does give a crude estimate of the effect. It is interesting to check the plausibility our results by comparing them with the analytic estimates of shot noise computed according to equations (16) and (24) in Yahil et al. (1991). For G15, and within a radius of $70\,h^{-1}$ Mpc, we obtain $\sigma_\delta{}^{\rm an.} = 0.42$ for the δ–δ case and $\sigma_v{}^{\rm int} = 1540\beta_c\,{\rm km\,s^{-1}}$ for the v_y–v_y one. Scaling to the $\beta_c = 0.21$ value of BP96, we obtain that in both cases the analytic shot noise is close to, although somewhat larger than, the scatter in the simulations. The explicit assumption made here is that the intrinsic scatter found in the mock simulation is representative for the real clusters too, and is independent of the other sources of error and the underlying field. The plausibility of these hypotheses will be assessed a posteriori when comparing the real cluster and POTENT fields.

As for the POTENT analysis (Section 2.1), the cluster velocity analysis has been limited to the supergalactic *Y* component, which is less prone to systematics. More extended mock catalogue analyses, based however on the distribution of *IRAS* galaxies, have demonstrated this point (Branchini et al. 1999). The other two Cartesian components are affected by systematic errors, arising from the cloning procedure that is used to fill the ZoA. Given the larger extent of the ZoA in the cluster case, we expect comparable, if not larger, systematics to affect the cluster velocity field. Correcting for this bias would require an error analysis based on more realistic Abell/ACO mock catalogues that are not currently available. Therefore, we restrict our analysis to a v_y–v_y comparison, under the working hypothesis that the *Y* component of the cluster velocity field is only affected by random errors.

3.4 Smoothed density and velocity fields

For the purpose of the comparison with POTENT, we compute smoothed density and velocity fields at the points of a cubic grid with spacing $5\,h^{-1}$ Mpc inside a box of side $320\,h^{-1}$ Mpc centred on the Local Group. We first generate 20 Monte Carlo realizations of our standard model as described above. To mimic the effect of observational errors and shot noise, we perturbed the cluster distances with a Gaussian noise of $150\,{\rm km\,s^{-1}}$. This value is slightly larger than the sum in quadrature of average observational and shot noise errors and corrects for the positive tail in the error distribution similar to the one observed in Fig. 2. The intrinsic error is not included here because it will enter implicitly when we later average over the 20 fields. A cloud-in-cell (CIC) scheme is used to translate the discrete cluster distribution into a density field at the grid points. The peculiar velocities at the grid points are recomputed from the reconstructed cluster distribution via linear GI+LB, with the force field smoothed by a small-scale top-hat window of radius $5\,h^{-1}$ Mpc. We minimize the scale of the top-hat force smoothing in order eventually to end up as close as possible to Gaussian smoothing on scales $\geqslant 12\,h^{-1}$ Mpc.

The 20 fields are then smoothed further with a Gaussian window of a larger radius $\sqrt{R_s^2 - R_1^2}$, where R_1 is the Gaussian smoothing radius equivalent in volume to the $5\,h^{-1}$ Mpc top-hat force smoothing. As mentioned already, we try three different smoothing scales, of $R_s = 12$, 15 and $20\,h^{-1}$ Mpc. These 20 fields are averaged to give the final smoothed fields used in the next section. Each of these 20 fields is affected by observational and shot noise errors. Moreover, as they represent 20 different Monte Carlo realizations of the cluster distribution for the same choice of parameters, we can account for the intrinsic errors by the very same averaging procedure. Indeed, the standard deviation over the 20 realizations represents the cumulative effect of intrinsic, observational and shot noise errors discussed in Section 3.3.1.

The only contribution left to the total error budget is the intrinsic scatter estimated in Section 3.3.2. This is modelled as Gaussian noise and is added in quadrature at each grid point. Therefore, the error estimates for the smoothed cluster fields, σ_{δ_c} and σ_{v_c}, are obtained by taking the standard deviation over the 20 catalogues and adding in quadrature a Gaussian noise of amplitude equal to the intrinsic scatter.

4 MEASURING β_c

We determine β_c in two different ways, via δ–δ and v_y–v_y comparisons. Because the δ–δ comparison is local, it avoids the incomplete sky coverage in the ZoA, but it uses only a small number of clusters (18 within $70\,h^{-1}$ Mpc). The v_y–v_y comparison, on the other hand, involves an integral over the cluster distribution in an extended volume, but it suffers from a large uncertainty caused by the unknown cluster distribution in the ZoA and beyond the edge of the sample. Therefore, the two methods are expected to suffer from different biases and can provide us with two estimates of β_c that are somewhat complementary.

We wish to restrict the quantitative comparison with the regions in space where both the errors in the cluster and POTENT fields are reasonably small. On the other hand, we wish to maximize the number of independent volumes compared, in order to minimize the cosmic scatter. We therefore need to optimize our choice of comparison volume, and test the robustness of the results to changes in this volume. The comparison volume has already been introduced in Section 2.1. The natural parameters for defining it the are the measure of poor sampling of the Mark III catalogue, R_4, our estimates of the random errors in the POTENT and cluster density fields (σ_{δ_p} and σ_{δ_c}) and the corresponding errors in the velocity fields (σ_{v_p} and σ_{v_c}). Our 'standard' cuts according to these parameters are reported in Table 1. As mentioned already in Section 2.1, we also impose a constraint on the misalignment angle between the cluster and POTENT velocity vectors. This serves as an additional classifier of 'good' points for the comparison, and helps us to avoid regions where we might have large, perhaps unaccounted for, errors. In our main analysis we restrict the comparison to points with a maximal misalignment angle of $\Delta\theta < 45°$. We later relax this constraint and verify the robustness of the results. We take the G15 smoothing as our standard case, with the above set of criteria defining our 'standard' comparison volume.

4.1 The β_c fitting method

The assumption underlying the β_c estimations is that the density and velocity fields recovered above are consistent with the model of GI+LB. In this framework the POTENT and the cluster fields are linearly related:

$$p = \beta_c c + A, \tag{4}$$

where p and c stand for the POTENT and cluster and represent either δ or the supergalactic Y velocity component. The cluster errors, σ_c, are comparable to the POTENT errors, σ_p. The best-fitting parameters are therefore obtained by minimizing the quantity

$$\chi^2 = \sum_{i=1}^{N_{tot}} \frac{(p_i - A - \beta_c c_i)^2}{(\sigma_{p,i}^2 + \beta_c^2 \sigma_{c,i}^2)}, \tag{5}$$

where the subscript i refers to any of the N_{tot} grid points within the comparison volume. As the fields have been smoothed on scales much larger then the grid separation, these points are, however, not independent. As in Hudson et al. (1995; see also Dekel et al. 1993), we estimate the effective number of independent points, N_{eff}, as

$$N_{eff}^{-1} = N_{tot}^{-2} \sum_{j=1}^{N_{tot}} \sum_{i=1}^{N_{tot}} \exp(-r_{ij}^2/2R_s^2), \tag{6}$$

where r_{ij} is the separation between grid points i and j. This expression weighs the dependent grid points, taking into account properly the finite comparison volume and its specific shape. This estimate is thus more accurate than the simplistic ratio of the comparison volume over the effective volume of the smoothing window, which assumes an infinite comparison volume. We account for the oversampling problem by using an effective χ^2 statistics defined by $\chi^2_{eff} \equiv (N_{eff}/N_{tot})\chi^2$, which is equivalent to multiplying the individual errors by the square root of the oversampling ratio N_{tot}/N_{eff}. The assumption we make is that this new statistics is approximately distributed like a χ^2 with N_{eff} degrees of freedom. In what follows we use it to assess the errors in β_c and A.

4.2 Testing the comparison

Before performing the comparisons with the real data, we wish to quantify further the possible systematics that might enter, verify the validity of the smoothing scheme adopted and find the optimal smoothing scale for the comparisons. Also, we would like to understand whether the intrinsic differences between the density and velocity field comparisons can affect the results. We do this by comparing the mock POTENT fields of Section 2.1 with the mock cluster ones from Section 3.3.2. The results of the density and velocity comparisons, within the standard comparison volume, for each of our three smoothing scales, are reported in Table 2. The values quoted in the table are all the mean values averaged over

Table 2. β_c from the POTENT versus cluster mock comparisons. Column 1: R_s, the smoothing radius in h^{-1} Mpc; column 2: N_{tot}, the number of grid points within the volume; column 3: N_{eff}, the effective number of independent volumes; column 4: R_e, the effective radius in h^{-1} Mpc; column 5: β_c^δ, β_c from δ–δ; column 6: σ_{β^δ}, the β_c^δ dispersion; column 7: A^δ, zero-point offset for δ–δ ; column 8: σ_A^δ, zero-point dispersion; column 9: $S^\delta \equiv \chi^2_{eff}/N_{eff}$ from δ–δ; column 10: β_c^v, β_c from v_y–v_y; column 11: σ_{β^v}, the β_c^v dispersion; column 12: A^v, zero-point offset for v_y–v_y; column 13: σ_A^v, zero-point dispersion; column 14: $S^v \equiv \chi^2_{eff}/N_{eff}$ from v_y–v_y.

R_s	N_{tot}	N_{eff}	R_e	β_c^δ	$\sigma^\delta_{\beta_c}$	A^δ	σ_A^δ	S^δ	β_c^v	$\sigma^v_{\beta_c}$	A^v	σ_A^v	S^v
12	694	10.4	27	0.31	0.10	0.00	0.07	0.93	0.27	0.10	−46	70	0.44
15	1644	12.4	37	0.32	0.13	0.02	0.06	0.91	0.30	0.13	−51	82	0.41
20	1823	7.2	38	0.26	0.27	0.02	0.05	0.98	0.28	0.19	−37	111	0.40

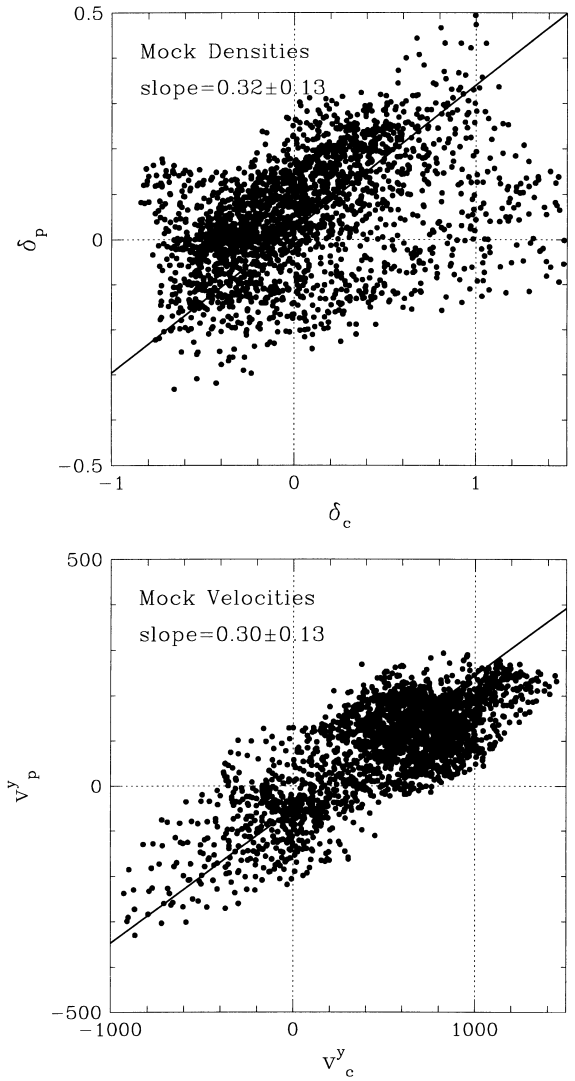

Figure 5. Comparing the mock POTENT and cluster fields. The averaged mock POTENT fields of Section 2.1 are compared with the mock cluster ones of Section 3.3.2, within the standard comparison volume. Top: $\delta-\delta$ comparison. Bottom: v_y-v_y comparison. The values quoted are the average over the 20 catalogues of β_c and its estimated error from the χ^2 fit. The solid lines represent the best-fitting averages.

the results of the 20 mock POTENT catalogues. The G15 case is illustrated in Fig. 5, where the average POTENT fields are compared to the cluster ones.

The values obtained for β_c in the G15 case are encouragingly close to the 'true' value of 0.31 (Section 3.3.2). The typical range of values obtained when altering the chosen volume for the comparison, from densities and velocities, lie in the range 0.26–0.35.

There are small differences for the other smoothings, with a tendency towards smaller β_c for the G20 case. All variations are, however, well within the formal $\chi^2_{\rm eff}$ error bars. In all cases, the zero-point found is hardly significant and is consistent with zero, within the error bars.

The $\chi^2/N_{\rm eff}$ values (defined as S in the table) are only slightly smaller than unity for the density comparisons, well within the accepted range given the small number of degrees of freedom (1 ± 0.4 for G15), but they are significantly smaller for the velocities. A similar trend was also found when comparing the POTENT fields with the true N-body ones. This may indicate that model velocities are more correlated than the scaling to $N_{\rm eff}$ obtained for the densities. If true, then our $\chi^2_{\rm eff}$ distribution deviates from that of a χ^2 with $N_{\rm eff}$ degrees of freedom, resulting in an error overestimate and in a $\chi^2/N_{\rm eff} < 1$ for velocities. Note that this effect is also associated with the application of the alignment constraint, and without it the value of χ^2 increases somewhat. So, perhaps for aligned vectors our errors are overestimated. Another, possibly not exclusive, explanation, which is also suggested by the POTENT versus N-body fields comparison, is the existence of systematic errors that do not average to zero.

The formal error bars obtained for β_c, in all cases, are significantly larger (by a factor of $\sim$2) than the spread of values obtained from the 20 Mark III mock catalogues. Again, this may suggest that our effective χ^2 statistic recovers the correct slope but overestimates the errors on β_c, and also for the $\delta-\delta$ comparison.

In summary, the important conclusion from the comparison of the mock data is that our method provides a fairly reliable estimate of β_c with no gross biases. The results are fairly robust to changes in the comparison volume and the smoothing scale. The reasonable χ^2 values obtained for the densities versus the too-low values for the velocities lead us to regard, here also, the density comparison as the more reliable one.

Our purpose is to constrain β_c in a meaningful way by comparing the density and velocity fields extracted from the cluster distribution with the fields recovered by POTENT from peculiar velocities. The competing obstacles are the very sparse sampling of the underlying density field by the clusters, on the one hand, and the limited volume sampled by peculiar velocities, on the other. The former dictates the use of a large smoothing scale, because small-scale structure is not traced properly by the clusters, while the latter calls for a relatively small smoothing scale, in order to minimize the cosmic scatter associated with the number of independent volumes, and the systematic biases in the method. The rough agreement between the results of different smoothings is encouraging. Large smoothing scales, such as the G20 case, are perhaps more pruned to systematics, and in any case, because they reduce the number of independent data points, they can only constrain β_c very weakly with large uncertainties. These considerations, along with the fact that it matches the intercluster separation, made us choose the G15 filter as our standard for the real data analysis. As mentioned before, the formal error bars from the $\chi^2_{\rm eff}$ statistics may overestimate the actual uncertainty in the results, but we conservatively choose to stick with these.

4.3 Visual comparison of maps

Fig. 6 displays the G15 density and velocity fields (in the CMB frame) from the clusters (left) and POTENT (right) reconstructions of the real data in three slices parallel to the supergalactic plane, within a sphere of radius $80\,h^{-1}$ Mpc about the Local Group. The densities and velocities of the clusters are scaled by $\beta_c = 0.21$. The heavy line delineates our standard comparison volume.

The similarity between the two density fields is evident in most regions. In both fields, the dominant features are the Great Attractor (on the left), the Perseus–Pisces supercluster (on the right), and the great void in between. On the other hand, the Coma supercluster, seen in the clusters map near $(X, Y) \approx (0, 70)$, is not reproduced at the same position in the POTENT map. Differences are also seen in the upper right quadrant of the $Z = -25\,h^{-1}$ Mpc plane.

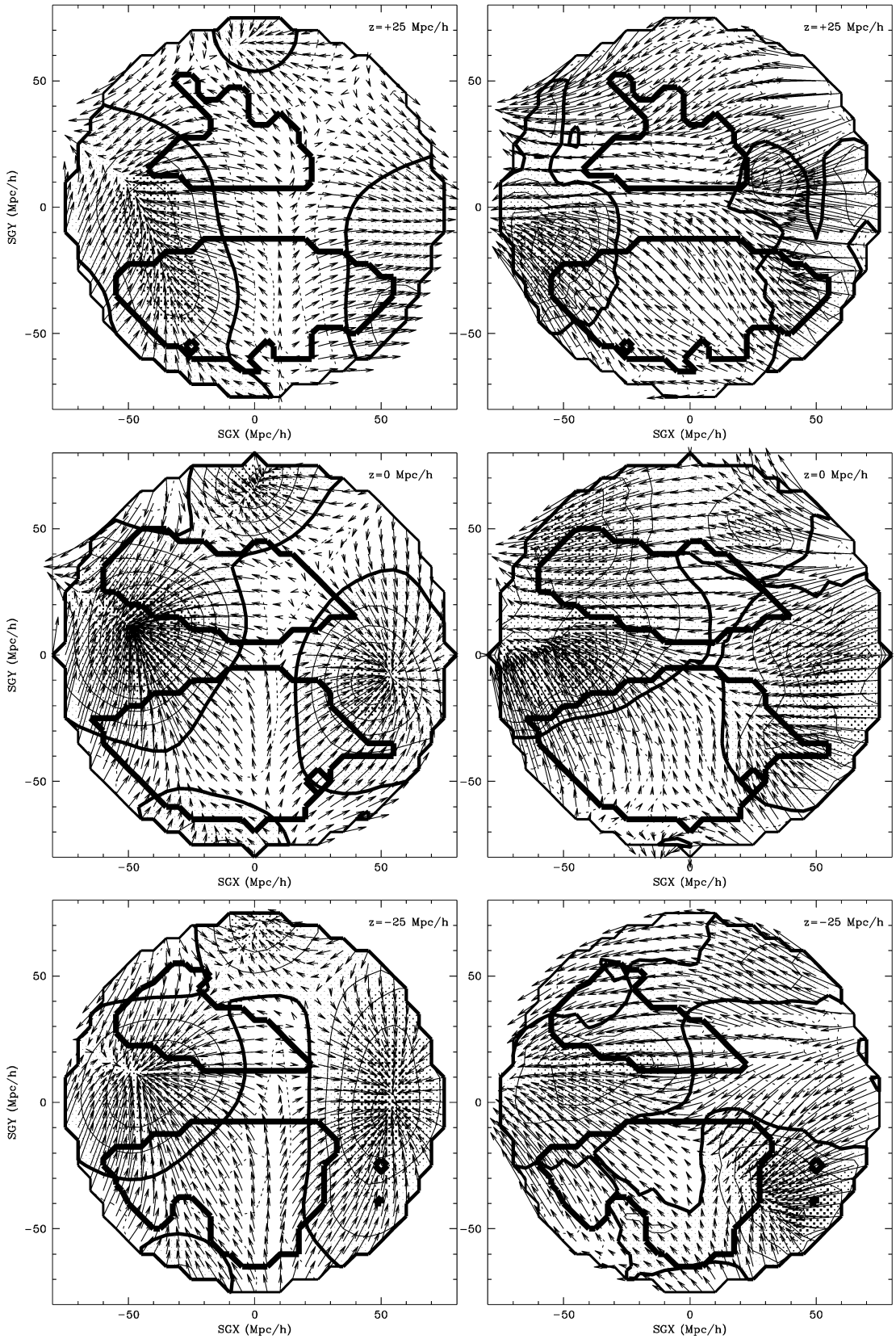

Figure 6. Density fluctuations and projected velocity field in supergalactic X–Y planes. The Mark III POTENT case is shown on the right and the cluster fields on the left, all G15 smoothed. The density contour spacing is $\Delta\delta = 0.15$; solid contours refer to overdense regions while dashed contours refer to negative overdensities. The thick line indicates the $\delta = 0$ contour. The heavy line defines the standard comparison volume. The lengths of the velocity vectors have been drawn on the scale of the plot. The cluster density fluctuations and velocities are scaled by $\beta_c = 0.21$. The top panel shows the plane defined by supergalactic $Z = +2500\,\mathrm{km\,s^{-1}}$, the middle panel shows *the* supergalactic plane of $Z = 0\,\mathrm{km\,s^{-1}}$, and the lower panel the plane defined by $Z = -2500\,\mathrm{km\,s^{-1}}$.

Table 3. β_c from the POTENT versus cluster real data comparisons. The symbols and units are the same as in Table 2. The first three rows refer to the standard comparison volume. The last two rows are for G15, when varying the comparison volume (see discussion in the text).

R_s	N_{tot}	N_{eff}	R_e	β_c^δ	$\sigma_{\beta_c}^\delta$	A^δ	σ_A^δ	S^δ	β_c^v	$\sigma_{\beta_c}^v$	A^v	σ_A^v	S^v
12	1239	11.7	33	0.21	0.06	−0.02	0.06	1.28	0.26	0.05	28	59	0.75
15	1855	10.6	38	0.20	0.07	−0.04	0.07	1.04	0.25	0.05	27	60	0.69
20	1537	5.0	36	0.22	0.12	−0.04	0.06	1.23	0.23	0.07	−4	83	0.58
15	1429	8.5	35	0.19	0.07	−0.04	0.07	1.00	0.26	0.06	22	67	0.73
15	4286	19.1	50	0.20	0.06	−0.02	0.04	1.01	0.26	0.05	9	48	1.06

There is also some qualitative agreement between the velocity fields, but it is less striking. The main features common to the two fields are the convergences into the Great Attractor and into Perseus–Pisces. The main difference is an additional bulk flow from right to left for the POTENT field, apparent in the three slices. Another feature absent in the POTENT field is the infall into Coma seen in the cluster field. Note that the main discrepancies lie outside the comparison volume, in regions where the errors are expected to be large at least in one of the reconstructions. These regions will be excluded from the quantitative comparison below.

It is also worth noticing that the density–velocity maps for the clusters are very similar to those obtained by Scaramella (1995b) from the same Abell/ACO cluster catalogues but using a somewhat different technique.

4.4 Estimating β_c by a density comparison

We perform the $\delta-\delta$ comparison within the standard volume. The errors in the POTENT field have been evaluated in Section 2.1, and for clusters we use the error estimates of Section 3.3. The results for the three smoothing radii are displayed in the first three rows of Table 3. For the preferred G15 case we find $\beta_c = 0.20 \pm 0.07$, and the best-fitting value stays essentially the same for the other cases (with the error bar increasing with the smoothing, owing to the smaller number of effective independent points). No significant zero-point offset is found in any of the cases. The $\delta-\delta$ scatter plot is displayed in Fig. 7 for the G15 case. The solid line is the best fit from the χ^2 minimization.

We have tried several variants of the comparison volume, in order to check the sensitivity of our results. Two representative examples are reported in the last two rows of Table 3. In the fourth case there we have considered the original standard volume but with a stricter R_4 cut, $R_4 < 10\,h^{-1}$ Mpc. The last column shows the results for the most interesting experiment, i.e. the one in which the misalignment constraint has been removed. The results of these tests all confirm the robustness of the $\beta_c \simeq 0.2$ value. For the density comparisons, we generally obtain $\chi^2_{eff}/N_{eff} \approx 1$, indicating a good fit. Note that relaxing the constraint on the misalignment angle more than doubles the number of grid points considered.

As outlined in Section 3.3.2, the present results have been obtained assuming that the scatter found in the mock cluster fields is representative of the intrinsic scatter in the real case and that it is independent of the other sources of error that form σ_{δ_c}. The resulting χ^2_{eff} values are an indication that these are indeed fair assumptions.

4.5 Estimating β_c by a velocity comparison

As already pointed out, it is important to perform the POTENT cluster regression for the velocities on the grounds of its complementarity with the δ analysis. Also, as we have already discussed in Section 3.3.2, we limit the comparison to the supergalactic Y component, which is the most robust component. We use the same minimizing procedure adopted in the $\delta-\delta$ comparison. The results are displayed in the right half of Table 3.

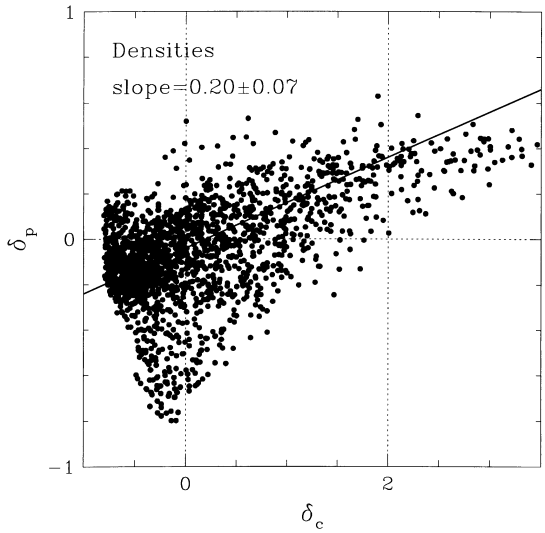

Figure 7. POTENT versus cluster G15 density field from the real data, at grid points within the comparison volume. The solid line results from the linear best fit.

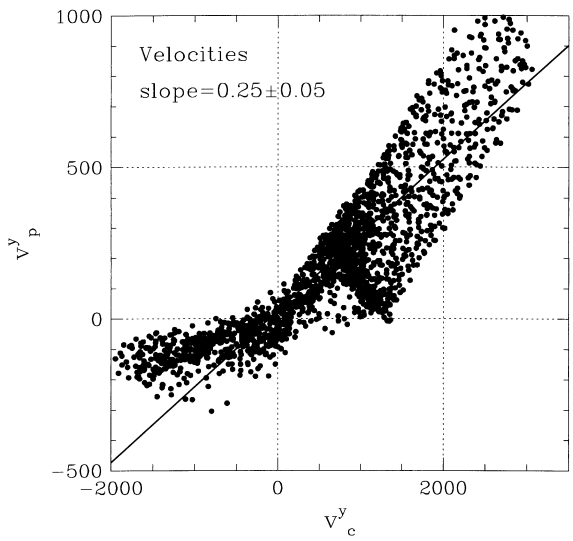

Figure 8. POTENT versus cluster G15 velocity field from the real data. Only the Y supergalactic components at grid points within the comparison volume are considered. The best-fitting line is also marked.

For our standard G15 case the result is now $\beta_c = 0.25 \pm 0.05$, somewhat higher than the density case, but still consistent within the error bars. The scatter plot for this case is shown in Fig. 8.

As was the case for the $\delta-\delta$ comparisons, no significant offset is detected, and the β_c value is quite robust for the different smoothing scales and under variations of the comparison volume (the changes in the resulting β are well below the 1σ significance level). Note again the peculiar morphology in the scatter plot, arising from the coherency in the peculiar velocities within independent cosmic structure. Although it may seem that the POTENT and cluster velocity fields differ in a large-scale bulk flow component, more quantitative, volume-limited comparisons performed by Branchini et al. (1996) and Branchini et al. (1999) have shown that the two bulk flows agree in amplitude and direction for a value of $\beta_c \approx 0.21$.

It is especially interesting to check the effect of removing the alignment constraint (the fifth case in the table). This is a demanding robustness check, because it extends the v_y-v_y comparison volume to points for which the velocity vectors can be severely misaligned. It is encouraging that, even in this case, the slope of the best-fitting line changes only by 4 per cent. The $\chi^2/N_{\rm eff}$ values lie somewhat below unity for all the cases explored except the one in which we have removed the alignment constraint. In this last case we obtain $\chi^2/N_{\rm eff} \approx 1$ both for the $\delta-\delta$ and v_y-v_y comparisons. A similar behaviour was also obtained for the mock comparisons (Section 4.2).

The errors $\sigma^v_{\beta_c}$ obtained from the real analysis are smaller than those obtained from the mock and listed in Table 2. Even accounting for the difference in the values of β_c, the two error estimates differ by a factor of $\approx$2. This mismatch probably arises from the characteristics of the mock velocity fields. Indeed, the small computational box used in the original K96 simulation and the constraint of having a vanishing bulk velocity on the scale of the box produce a remarkably quiet velocity field with a bulk velocity of only $100\,{\rm km\,s^{-1}}$, already on a scale of $40\,h^{-1}\,$Mpc. This velocity field has been used to estimate the POTENT and some of the cluster velocity errors. Real velocities, however, are larger than the mock ones and these uncertainties probably underestimate the errors for the real case, leading to the smaller $\sigma^v_{\beta_c}$ value listed in Table 3.

The v_y-v_y comparison described above has been performed in the CMB reference frame. Predicting velocities from galaxy redshift surveys is commonly done though in the LG frame, in order to minimize the influence of mass concentrations from outside the sample volume. The LG frame might therefore be considered the natural frame in which to perform comparisons with reconstructed velocities. In our case, the velocities are reconstructed from the far-extending cluster catalogue, which alleviates the above problem, and we regard a CMB comparison as reliable. Furthermore, performing the comparison in the LG frame would introduce extra complexities, requiring a somewhat ad hoc transformation to a common LG frame for both the cluster and POTENT velocity fields. As a crude test of the sensitivity of our results to changes in the framework of reference, we shift both velocity fields to the cluster LG frame, as defined by the smoothed cluster velocity at the origin (with a reasonable choice for β_c). Alternatively we consider the peculiar velocities relative to the central observer of each reconstructed velocity field independently. The standard G15 comparison of the Y components gives $\beta_c = 0.24 \pm 0.05$ and 0.25 ± 0.04 respectively, for these two cases, demonstrating once more the robustness of our result.

5 CONCLUSIONS

We have used the smooth matter fluctuation field obtained by applying the POTENT machinery to the Mark III data set and compared it with the density field deduced from the Abell/ACO cluster distribution. A similar comparison has also been performed between the reconstructed cluster velocities and those from the Mark III catalogue, smoothed on the same scale. We have performed a careful error analysis using mock galaxy and cluster catalogues derived from N-body simulations. The mock catalogues used in our POTENT error analysis were especially designed to reproduce the Mark III characteristics. Uncertainties in the cluster fields, on the other hand, were evaluated using a hybrid procedure that extends the Monte Carlo error analysis of BP96 and is complemented by a similar approach to the POTENT mock catalogue analysis.

Cluster and POTENT fields show remarkable similarities within $70\,h^{-1}\,$Mpc, while their major discrepancies are usually confined to regions where the cluster or POTENT reconstructions are known to be unreliable. Quantitative comparisons between cluster and POTENT fields have been performed in an attempt to estimate the cluster β parameter. The results are quite robust and for the standard G15 case we find $\beta_c = 0.20 \pm 0.07$ from the $\delta-\delta$ regression, and a somewhat larger value of $\beta_c = 0.25 \pm 0.05$ from the v_y-v_y case. This systematic discrepancy is within the 1σ significance level, but it is present in all the cases explored. We therefore choose to quote a joint estimate for β_c of 0.22 ± 0.08.

Some differences between the two values are not unexpected given the different nature of the comparisons. A similar regression based on the mock catalogues showed that some discrepancies do exist. However, in the mock tests the difference between the two values was of smaller magnitude and in the opposite direction. The different trends between the real and mock results could arise from the different modelling of the mass distribution outside the sampled regions, which can affect the cluster velocity field. There are other indications for regarding the $\delta-\delta$ results as more reliable. The $\chi^2/N_{\rm eff}$ values for the density comparison were around unity, while systematically lower values were obtained for the velocities. Also the POTENT velocity field was found in the mock catalogue analysis to suffer from more biases.

The present analysis suggests a value of $\beta_c \simeq 0.20$–0.25 for clusters, in accordance with previous estimates. The distribution of clusters is expected to be biased with respect to the distribution of galaxies with a biasing factor $b_{cg} \simeq 3$–4 (e.g. from the different correlation lengths obtained for clusters and for galaxies – Bahcall & Soneira 1983; Huchra et al. 1990). Peacock & Dodds (1994) find such values for the biasing factors, derived from the ratios of power spectra calculated for different data sets. Their quoted relative biasing factors for Abell clusters, radio galaxies, optical galaxies and *IRAS* galaxies is 4.5:1.9:1.3:1, respectively. Recent results from a comparison of the cluster density and velocity fields with the fields recovered from the PSCz redshift survey constrain this parameter to $b_{cg} = 4.4 \pm 0.6$, with respect to *IRAS* galaxies (Branchini et al. 1999). Together with our constraint on β_c, this implies $\beta_I \sim 1$ with, however, a 1σ uncertainty of $\sim$50 per cent. Although our analysis cannot provide us with a firm β_c determination, because of the large uncertainties associated with the $\delta-\delta$ and v_y-v_y comparisons, it leads toward a value of β_c that is consistent with an Einstein–de Sitter universe for a reasonable cluster linear bias parameter of $b_c \sim 4.5$. Our value of b_c is a linear fit to the $\delta-\delta$ and v_y-v_y scatter plots. Under the assumption of linear biasing, b_c represents the relative biasing of Abell/ACO

clusters with respect to the underlying mass density field. Linear biasing, however, does not need to be a good approximation for clusters, because the large value of b_c causes the LB hypothesis to break down in those regions where $\delta < -b_c^{-1}$. Methods to measure the degree of non-linearity in the biasing relation have recently been developed and applied to galaxy distributions (e.g. Sigad, Dekel & Branchini 1999; Somerville et al. 2000; Narayanan et al. 1999) but not yet to clusters of galaxies. However, there is indirect evidence of the small deviation from linear biasing. The first piece of evidence comes from the visual inspection of the $\delta-\delta$ scatter plot in Fig. 7, which does not deviate appreciably from LB expectations (the linear fit). A more convincing piece of evidence of the small deviations from the LB approximation is obtained by performing the $\delta-\delta$ comparison for various smoothing filters. Increasing the smoothing length decreases the amplitude of density fluctuations and reduces the size of those regions in which the constraint $\delta < -b_c^{-1}$ causes the LB model to fail. As shown in Table 2, increasing the smoothing radius from 12 to $20\,h^{-1}$ Mpc does not change β_c^δ significantly, showing that regions where LB does not apply play little role in our analysis. As a consequence, and for all practical purposes, linear biasing is a good approximation on the scales relevant for our analysis and therefore we can regard b_c as the biasing parameter for Abell/ACO clusters.

ACKNOWLEDGMENTS

We thank the referee Michael Strauss for his helpful comments and suggestions. We are grateful to Ami Eldar for his help in applying POTENT to the mock catalogues, Tsafrir Kolatt for providing the mock simulation and catalogues and Yahir Sigad for helpful discussions. MP and EB warmly thank Bepi Tormen for providing his grouped version of the Mark II catalogue, which was used in some of the preliminary work. EB has been supported by an EEC *Human Capital and Mobility* fellowship and acknowledges the hospitality of the Hebrew University, where this work was completed. IZ acknowledges supports by the DOE and the NASA grant NAG 5-7092 at Fermilab.

REFERENCES

Abell G. O., 1958, ApJS, 3, 211
Abell G. O., Corwin H. G., Olowin R. P., 1989, ApJS, 70, 1
Bahcall N. A., Soneira R. M., 1983, ApJ, 270, 20
Branchini E., 1995, PhD thesis, International School of Advanced Studies, Trieste
Branchini E., Plionis M., 1995, in Maurogordato S., Balkowski C., Tao C., Trân Thanh Vân J., eds, Proc. Moriond Astrophysics Meeting on Clustering in the Universe. Editions Frontieres, Gif-sur-Yvette, p. 277
Branchini E., Plionis M., 1996, ApJ, 460, 569 (BP96)
Branchini E., Plionis M., Sciama D. W., 1996, ApJ, 461, L17
Branchini E. et al., 1999, MNRAS, 308, 1
da Costa L. N., Nusser A., Freudling W., Giovanelli R., Haynes M. P., Salzer J. J., Wegner G., 1998, MNRAS, 299, 425
Davis M., Nusser A., Willick J., 1996, ApJ, 473, 22
Dekel A., 1994, ARA&A, 32, 371
Dekel A., 1997, in da Costa L. N., Renzini A., eds, Galaxy Scaling Relations. Springer, Berlin-Heidelberg, p. 245
Dekel A., 1998, in Dekel A., Ostriker J. P., eds, Formation of Structure in the Universe. Cambridge Univ. Press, Cambridge, p. 250
Dekel A., Lahav O., 1999, ApJ, 520, 24
Dekel A., Blumenthal G. R., Primack J. R., Olivier S., 1989, ApJ, 338, L5
Dekel A., Bertschinger E., Faber S. M., 1990, ApJ, 364, 349 (DBF)
Dekel A., Bertschinger E., Yahil A., Strauss M., Davis M., Huchra J., 1993, ApJ, 412, 1
Dekel A., Eldar A., Kolatt T., Yahil A., Willick J. A., Faber S. M., Courteau S., Burstein D., 1999, ApJ, 522, 1 (D99)
Giovanelli R., Haynes M. P., Wegner G., da Costa L. N., Freudling W., Salzer J. J., 1996, ApJ, 464, L99
Giovanelli R., Haynes M. P., Herter T., Vogt N., da Costa L. N., Freudling W., Salzer J. J., Wegner G., 1997, AJ, 113, 22
Giovanelli R., Haynes M., Freudling W., da Costa L., Salzer J., Wegner G., 1998a, ApJ, 505, L91
Giovanelli R., Haynes M., Salzer J., Wegner G., da Costa L., Freudling W., 1998b, AJ, 116, 2632
Huchra J. P., Henry J. P., Postman M., Geller M. J., 1990, ApJ, 365, 66
Hudson M. J., 1994, MNRAS, 266, 468
Hudson M. J., Dekel A., Courteau S., Faber S. M., Willick J. A., 1995, MNRAS, 274, 305
Juskiewicz R., Vittorio V., Wyse R. F. G., 1990, ApJ, 349, 408
Katgert P. et al., 1996, A&A, 310, 8
Kolatt T., Dekel A., Ganon G., Willick J. A., 1996, ApJ, 458, 419 (K96)
Lahav O., Nemiroff R. J., Piran T., 1990, ApJ, 350, 119
Lauer T. R., Postman M., 1994, ApJ, 425, 418
Mazure A. et al., 1996, A&A, 310, 31
Narayanan V., Weinberg D., Branchini E., Frank C., Maddox S., Oliver S., Rowan-Robinson M., Saunders W., 1999, ApJ, submitted
Peacock J. A., Dodds S. J., 1994, MNRAS, 267, 1020
Plionis M., 1995, in Maurogordato S., Balkowski C., Tao C., Trân Thanh Vân J., eds, Proc. Moriond Astrophysics Meeting on Clustering in the Universe. Editions Frontieres, Gif-sur-Yvette, p. 273
Plionis M., Valdarnini R., 1991, MNRAS, 249, 46 (PV91)
Plionis M., Kolokotronis V., 1998, ApJ, 500, 1
Scaramella R., 1995a, in Maurogordato S., Balkowski C., Tao C., Trân Thanh Vân J., eds, Proc. Moriond Astrophysics Meeting on Clustering in the Universe. Editions Frontieres, Gif-sur-Yvette, p. 257
Scaramella R., 1995b, Astrophys. Lett. Commun., 32, 137
Scaramella R., Vettolani G., Zamorani G., 1991, ApJ, 376, L1
Sigad Y., Dekel A., Eldar A., Strauss M., Yahil A., 1998, ApJ, 495, 516 (PI98)
Sigad Y., Dekel A., Branchini E., 2000, ApJ, submitted
Somerville R., Lemson G., Sigad Y., Dekel A., Kauffmann G., White S., 2000, MNRAS, submitted
Strauss M. A., Willick J. A., 1995, Phys. Rep., 261, 271
Tormen G., Moscardini L., Lucchin F., Matarrese S., 1993, ApJ, 411, 16
Van Haarlem M., Frenk C. S., White S. D. M., 1997, MNRAS, 287, 817
Willick J. A., Strauss M. A., 1998, ApJ, 507, 64
Willick J. A., Courteau S., Faber S. M., Burstein D., Dekel A., 1995, ApJ, 446, 12
Willick J. A., Courteau S., Faber S. M., Burstein D., Dekel A., Kolatt T., 1996, ApJ, 457, 460
Willick J. A., Courteau S., Faber S. M., Burstein D., Dekel A., Strauss M., 1997a, ApJS, 109, 333
Willick J. A., Strauss M. A., Dekel A., Kolatt T., 1997b, ApJ, 486, 629
Yahil A., Strauss M. A., Davis M., Huchra J. P., 1991, ApJ, 372, 380

This paper has been typeset from a TEX/LATEX file prepared by the author.